Biophysical Journal
Article

Biophysical Society

# Stabilization of the Activated hERG Channel Voltage Sensor by Depolarization Involves the S4-S5 Linker

Samrat Thouta,[1] Christina M. Hull,[1] Yu Patrick Shi,[1] Valentine Sergeev,[1] James Young,[1] Yen M. Cheng,[1] and Thomas W. Claydon[1,*]

[1]Department of Biomedical Physiology and Kinesiology, Simon Fraser University, Burnaby, British Columbia, Canada

ABSTRACT Slow deactivation of hERG channels is critical for preventing cardiac arrhythmia yet the mechanistic basis for the slow gating transition is unclear. Here, we characterized the temporal sequence of events leading to voltage sensor stabilization upon membrane depolarization. Progressive increase in step depolarization duration slowed voltage-sensor return in a biphasic manner ($\tau_{fast}$ = 34 ms, $\tau_{slow}$ = 2.5 s). The faster phase of voltage-sensor return slowing correlated with the kinetics of pore opening. The slower component occurred over durations that exceeded channel activation and was consistent with voltage sensor relaxation. The S4-S5 linker mutation, G546L, impeded the faster phase of voltage sensor stabilization without attenuating the slower phase, suggesting that the S4-S5 linker is important for communications between the pore gate and the voltage sensor during deactivation. These data also demonstrate that the mechanisms of pore gate-opening-induced and relaxation-induced voltage-sensor stabilization are separable. Deletion of the distal N-terminus (Δ2–135) accelerated off-gating current, but did not influence the relative contribution of either mechanism of stabilization of the voltage sensor. Lastly, we characterized mode-shift behavior in hERG channels, which results from stabilization of activated channel states. The apparent mode-shift depended greatly on recording conditions. By measuring slow activation and deactivation at steady state we found the "true" mode-shift to be ~15 mV. Interestingly, the "true" mode-shift of gating currents was ~40 mV, much greater than that of the pore gate. This demonstrates that voltage sensor return is less energetically favorable upon repolarization than pore gate closure. We interpret this to indicate that stabilization of the activated voltage sensor limits the return of hERG channels to rest. The data suggest that this stabilization occurs as a result of reconfiguration of the pore gate upon opening by a mechanism that is influenced by the S4-S5 linker, and by a separable voltage-sensor intrinsic relaxation mechanism.

## INTRODUCTION

The human ether-á-go-go related gene (hERG) encodes the pore-forming α-subunit of the cardiac rapid delayed rectifier potassium current, $I_{Kr}$. This current contributes to cardiac repolarization and consequently normal cardiac excitability and rhythm. Upon membrane depolarization, hERG channels activate slowly and inactivate rapidly, but upon repolarization, channels recover from inactivation into the open state. Slow deactivation of open channels produces a resurgent repolarizing current that aids termination of the cardiac action potential. Despite the critical role in determining cardiac excitability, the molecular basis of slow hERG channel deactivation is currently unclear.

Like other voltage-gated $K^+$ (Kv) channels, hERG channels are a tetrameric assembly of six α-helical transmembrane segments (S1–S6), with S1–S4 forming the voltage sensing domain, which transitions between resting and activated states in response to membrane depolarization, and S5-S6 forming the conducting pore domain. Numerous studies support a role for the hERG S4-S5 linker in transducing voltage sensor motions to the pore gate (1–5); however, recent structural (6) and functional (7) evidence suggests that voltage sensing may be coupled to the pore in hERG by an alternate mechanism that is divergent from *Shaker*-like Kv channels.

Activation and deactivation pathways in hERG, and other channels, are not symmetrical, but rather exhibit hysteresis, or mode-shift behavior, where the energy landscape during deactivation is different from that during activation. This results in a separation of the voltage dependencies of activation and deactivation such that more energy is required to return channels to the deactivated state than to activate them (2,8–13). Stabilization or immobilization of voltage sensor charges has been observed in a number of channels in response to depolarization and this can be mediated by

*Submitted September 9, 2016, and accepted for publication December 15, 2016.*

*Correspondence: thomas_claydon@sfu.ca

Samrat Thouta and Christina M. Hull contributed equally to this article.

Editor: William Kobertz.

http://dx.doi.org/10.1016/j.bpj.2016.12.021

factors outside of the voltage sensor, such as the N-type inactivation particle or other intracellular pore blockers that prevent closure of the pore gate (14,15), the permeant ion species (16), or inactivation (17,18). Recent studies in *Shaker*, Kv1.2, and Kv3.1 channels, as well as the voltage-sensitive phosphatase, Ci-VSP, have suggested that sustained depolarization also induces an intrinsic reconfiguration of the voltage sensor into a "relaxed" state that stabilizes the activated state (19–21). These studies propose that relaxation retards return of the voltage sensor during deactivation resulting in mode-shift behavior. The mechanistic basis of relaxation is unclear, but its presence in WT Ci-VSP (which comprises a voltage sensor domain, but no pore domain or inactivation process, both with and without its phosphatase load) has been interpreted to indicate that relaxation is an intrinsic property of the voltage sensor (21). In support of this idea, voltage sensor relaxation in *Shaker* is also sensitive to both the length and composition of the S3-S4 linker (22). Other studies have shown that mutations in the S4-S5 linker and S6 of *Shaker* channels, which uncouple the voltage sensor from the pore gate, also impede mode-shift behavior, suggesting that mode-shift might originate from the mechanical load placed on the voltage sensor domain by the pore (23,24). Others have also suggested that voltage-independent gating steps might underlie mode-shift behavior, rather than voltage sensor-mediated relaxation (25). Importantly, a recent study (19) demonstrated in *Shaker* and Kv1.2 channels that stabilization of the activated voltage sensor due to pore opening can be kinetically separated from that due to relaxation of the voltage sensor. More recently, Labro et al. (26), observed a very rapid component of charge stabilization in Kv3.1 channels, which kinetically preceded pore gate opening, and was attributed by the authors to an "ultra-fast" relaxation mechanism. These studies emphasize the presence of a stabilization of the activated voltage sensor being an intrinsic property of the voltage sensing unit, but the mechanistic basis underlying relaxation is currently illusive.

Despite the physiological importance of slow deactivation in hERG channels, relaxation of the voltage sensor and stabilization of the activated voltage sensor by the pore in the control of deactivation has largely been overlooked in these channels. Two recent studies investigating the effects of the N-terminal domain on hERG mode-shift behavior (10,13) reported differing effects, leaving questions regarding the role of the N-terminus in stabilizing activated voltage sensor charges and the sequence of events that leads to retardation of deactivation and mode-shift behavior.

This study aims to better understand the control of hERG channel deactivation by characterizing hERG gating currents and ionic currents during prolonged voltage steps that allow for measurement of activation and deactivation and on- and off-gating charge under steady-state conditions. Using several mutations as tools, we define key steps in the deactivation pathway that limit voltage sensor return to produce the physiologically relevant resurgent hERG current in cardiomyocytes.

## MATERIALS AND METHODS

### Molecular biology

Wild-type (WT) and mutant hERG channel constructs were prepared for expression in *Xenopus laevis* oocytes as described in Cheng et al. (27).

### Oocyte preparation and injection

Oocytes were isolated from female *Xenopus laevis* frogs and injected with WT or mutant hERG cRNA in accordance with the Simon Fraser University Animal Care Committee, and Canadian Council on Animal Care protocols and procedures and as described in Cheng et al. (27).

### Electrophysiology

Whole-cell membrane current recordings from oocytes expressing WT or mutant hERG constructs were collected using two-electrode voltage-clamp with an OC-725C amplifier (Warner Instruments, Hamden, CT). Signals were digitized and acquired using a Digidata 1440 A/D convertor and pClamp 10.2 software (Axon Instruments, Foster City, CA). Recordings were performed at room temperature (20–22°C) while oocytes were perfused with ND96 solution (96 mM NaCl, 3 mM KCl, 0.5 mM $CaCl_2$, 1 mM $MgCl_2$, and 5 mM HEPES, titrated to pH 7.4 with NaOH) at 1 mL/min. Reagents were purchased from Sigma-Aldrich (St. Louis, MO). Recording microelectrodes were made from thin-walled borosilicate glass (World Precision Instruments, Sarasota, FL) with a resistance of 0.2–2.0 MΩ when filled with 3 M KCl. Current signals were digitized at a 10 kHz sampling frequency and low-pass filtered at 4 kHz (Bessel filter). Gating current recordings were collected using the Vaseline gap cut-open voltage-clamp technique with a CA-1B amplifier (Dagan, Minneapolis, MN) and recorded using PATCHMASTER software (ITC-16 interface; HEKA Electronik, Bellmore, NY) as described in Thouta et al. (28). The hERG blocker terfenadine (20 $\mu$M) was added to both external and internal solutions to inhibit ionic current. Before gating current recordings, the membrane was held at −10 mV for ~30 min to aid $K^+$ depletion from the cytosol to reduce the driving force for residual ionic currents. Recording microelectrodes were made from thin-walled borosilicate glass with a resistance of 250–500 KΩ when filled with 3 M CsCl. Capacitative currents were compensated using the analog circuitry of the amplifier. Linear leak subtraction was performed online using a P/-8 protocol. Typical non-leak-subtracted WT hERG gating current records and examples of recordings from uninjected oocytes are shown in Fig. S1 in the Supporting Material.

### Data analysis

Data were analyzed using Clampfit 10.3 (Axon Instruments), SigmaPlot11 (Systat Software, San Jose, CA), or IGOR Pro (WaveMetrics, Lake Oswego, OR) software. Steady-state conductance-voltage (GV) relationships were obtained from peak tail currents. Charge versus voltage (QV) relationships for activation and deactivation were obtained by integrating off-gating currents at −100 mV, or on-gating currents at 0 mV, respectively. Calculated integrals were normalized to the total charge moved and were plotted as a function of the preceding test pulse voltage. GV and QV curves were fitted with the Boltzmann equation: $y = 1/(1 + \exp(V_{1/2}–V)/k)$, where $y$ is the relative conductance or charge movement, normalized to maximum conductance ($G/G_{max}$) or charge movement ($Q/Q_{max}$), $V_{1/2}$ is the voltage at which half maximal conductance was recorded or half of the total charge had moved, $V$ is the test voltage, and $k$ is the slope factor. Ionic current deactivation and off-gating current kinetics were fitted with a double

exponential function yielding fast and slow components. We report the fast time constant for ionic current deactivation because current decay at −110 mV was dominated (>85%) by the fast component, which did not change appreciably in any of our experiments. For off-gating currents, we report the weighted $\tau$, which expresses the fast and slow components of current decay weighted according the relative amplitude of each component, as a simplified best-approach for the quantification of the biexponential off-gating current (Fig. S2). This approach was taken, because the mechanistic basis for the two components is unclear, and because the relative amplitude of the two components changed with depolarizing step duration (Fig. S2). Unless otherwise noted, data are expressed as mean ± SE. The value $n$ represents the number of oocytes tested. In figures, arrows indicate the zero current level.

## RESULTS

### Prolonged depolarization stabilizes the activated hERG voltage sensor

hERG channel deactivation kinetics are characteristically slow, but the mechanistic basis for this is unclear. Moreover, previous evidence suggests that hERG channels follow a different energetic pathway during deactivation from that during activation resulting in a mode-shift (2,10,13), but this pathway has not been characterized. We sought to better understand the deactivation pathway in hERG channels by exploring the transition of activated channels to deactivated states that results in mode-shift behavior. Fig. 1 shows the effects of the duration of depolarization on the kinetics of hERG channel pore closure during deactivation. Depolarizing steps to different voltages and of variable duration were applied to activate channels followed by a test pulse to −110 mV to deactivate channels. Typical ionic current traces (Fig. 1 *A*) recorded in response to this voltage protocol show that deactivation, which at −110 mV is dominated by a fast component, slowed as the duration of the depolarizing step was increased. This slowing is highlighted in Fig. 1 *B* by the scaled deactivation traces recorded after 50, 500, and 15,000 ms depolarizing steps to +60 mV. Fig. 1 *C* shows the time constant of channel deactivation plotted against the duration of the depolarizing pulse. These data, from experiments using three different depolarizing voltages, show that increasing the duration of the depolarization step slows hERG channel deactivation kinetics. In each case, the relationship could be fitted with a biexponential function with the two phases of slowing yielding $\tau$-values of 93 ± 5 ms (relative amplitude 0.42 ± 0.03) and 4.3 ± 0.5 s (relative amplitude 0.58 ± 0.03) with a depolarization to +60 mV ($n = 6$).

A similar biphasic slowing of deactivation has been observed in *Shaker* and Kv1.2 channels where the fast phase correlated with the kinetics of pore opening (19). Although the kinetics of the faster phase of hERG deactivation slowing shown in Fig. 1 *C* are an order-of-magnitude slower than reported for *Shaker* and Kv1.2 (19), they approximated the time course of the relatively slow activation of hERG channels measured from envelope-of-tails experiments (5). This correlation suggests that rearrangements of the hERG pore gate during activation retard pore closure. The more delayed component of deactivation slowing in Fig. 1 *C* occurred in response to more prolonged depolarizations that exceeded the time course of pore opening. It is interesting that this slower deactivation delay in hERG channels occurred with kinetics that are similar to those reported in *Shaker* and Kv1.2 channels (19), despite the marked difference in the kinetic properties of both activation and inactivation in hERG channels.

To understand the mechanistic basis of slowed channel deactivation as a result of depolarization in hERG channels, on- and off-gating charge was measured from voltage sensor-gating current recordings. Fig. 2 *A* shows a typical WT hERG gating current record in response to a 250 ms

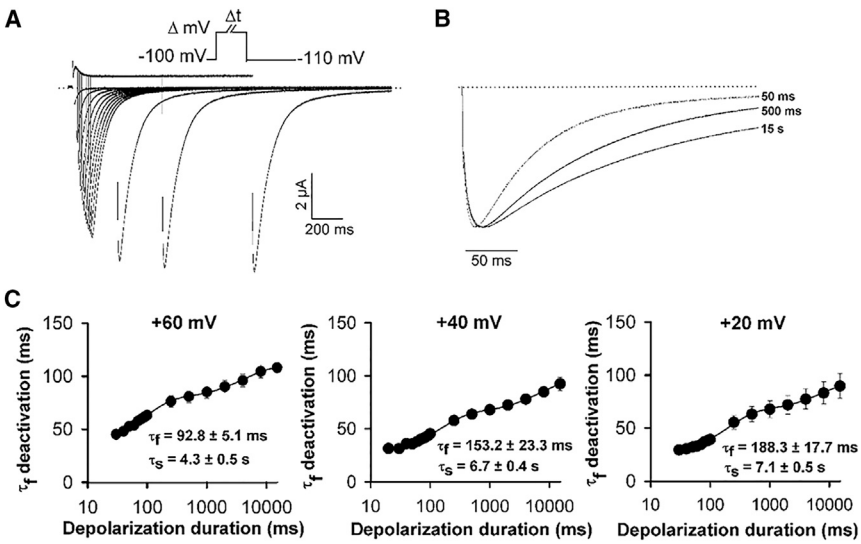


FIGURE 1 Prepulse-dependent slowing of WT hERG channel deactivation. (*A*) Typical current traces from WT channels recorded in response to the protocol shown in which the depolarizing test pulse (+60 mV) duration ($\Delta t$, in ms) was varied. (*B*) Superposition of normalized ionic deactivation tail current traces from (*A*), recorded at −110 mV after 50, 500, and 15,000 ms steps to +60 mV to highlight the change in deactivation. (*C*) Plot of mean $\tau$-fast component of deactivating current ($\tau_f$ deactivation) as a function of increasing depolarization duration at +60, +40, and +20 mV. Data were fitted to a double exponential function ($n = 6$, 5, and 4, respectively).

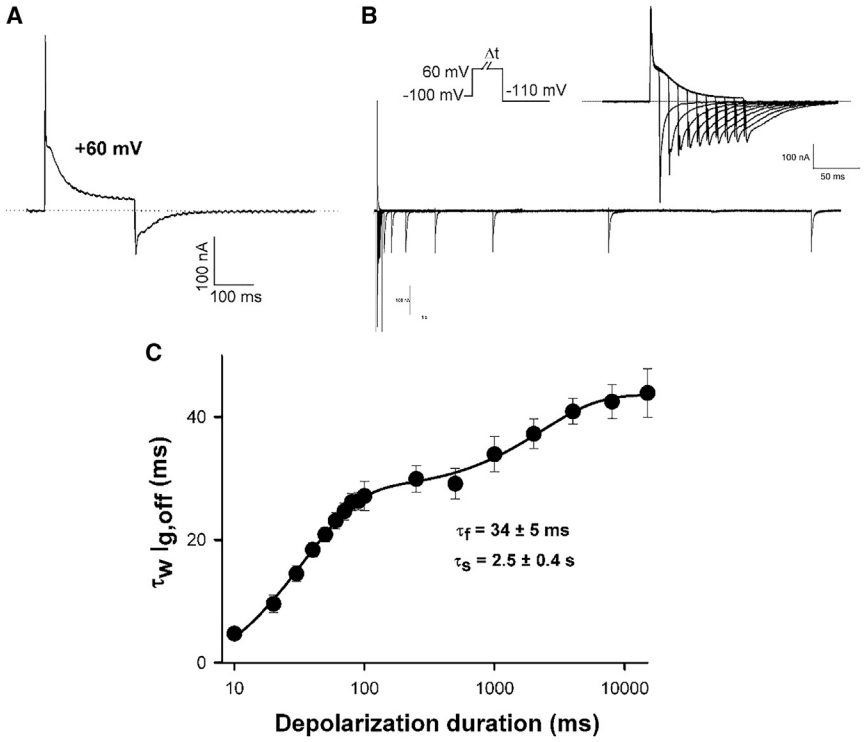


FIGURE 2 Stabilization of the hERG-activated voltage sensor by prolonged depolarization. (*A*) Typical hERG WT gating current traces recorded in response to a 250 ms step depolarization to +60 mV from a holding potential of −100 mV. (*B*) Typical hERG gating current traces recorded in response to the protocol shown in which the depolarizing test pulse duration was varied. (*Inset*) Currents following shorter durations on an expanded timescale to highlight the off-gating current decays. (*C*) Plot of the mean weighted $\tau$ of the off-gating current ($\tau_w I_{g,off}$) as a function of increasing depolarization duration at +60 mV. Data were fitted to a double exponential function ($n = 6$).

step depolarization to +60 mV, which highlights the complex kinetics associated with charge transit across the membrane as has been reported previously in these channels (11,28–31). Both on- and off-gating currents display pronounced fast and slow phases of decay. Fig. 2 *B* shows on- and off-gating current recordings in response to a +60 mV depolarizing step of varying duration followed by a repolarizing step to −110 mV. Off-gating kinetics depended greatly on the duration of the depolarizing step. Fig. 2 *C* shows a plot of the weighted $\tau$ of off-gating charge against depolarizing step duration, which revealed a biexponential relationship that could be described with $\tau$-values of 34 ± 5 ms (relative amplitude 0.54 ± 0.02) and 2.5 ± 0.4 s (relative amplitude 0.46 ± 0.02; $n = 6$). This dependence of the kinetics of voltage sensor return upon depolarization duration is qualitatively similar to the ionic current measurements of channel deactivation in Fig. 1. Together, these data suggest that slowed deactivation gating in response to prolonged depolarization occurs as a result of stabilization of the voltage sensor in the activated configuration.

## Perturbation of the S4-S5 linker disturbs communication of the state of the pore gate to the voltage sensor during deactivation

We have previously shown that sites within the S4-S5 linker profoundly influence the open-closed equilibria in hERG channels. Mutation of one site in particular, G546, left-shifts the voltage-dependence of activation gating by ~50 mV, suggesting that flexibility of the connecting linker stabilizes closed channel states during activating voltage steps (5). Interestingly, we found here that the G546L mutation impeded the influence of the pore on the stability of the activated hERG voltage sensor pore during repolarization. Fig. 3 shows the dependence of ionic current deactivation and voltage sensor off-gating current upon the duration of the depolarizing step applied to G546L channels. The relationship between deactivation rate and depolarizing step duration was no longer biphasic in the mutant channels, but could be described by a single exponential ($n = 6$). This same effect was observed in measurements of the slowing of off-gating with increasing depolarizing step duration, which could also be fitted with a single exponential function ($n = 5$). The data show that the fast phase of slowing of pore closure and gating charge return, which in WT channels is associated with channel opening, was no longer prominent in G546L channels. Significant slowing of channel deactivation in the mutant channels only occurred after durations much longer than the time course of channel opening (~43 ms (5)). These data suggest that the depolarization-induced stabilization of the activated voltage sensor position by the open pore gate and voltage sensor relaxation are separable. The G546L mutation apparently impedes the faster phase of off-gating current slowing that is due to stabilization of the voltage sensor by the open pore gate while leaving the relaxation-induced stabilization of the activated voltage sensor and open pore intact.

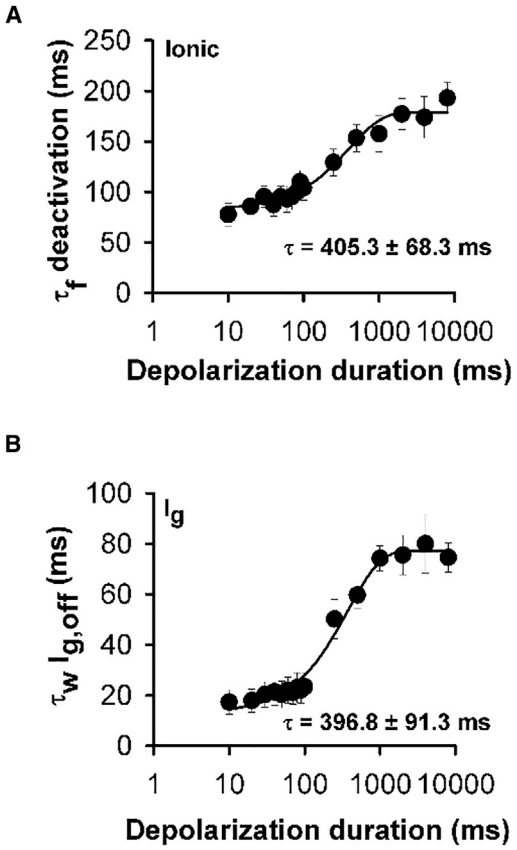


FIGURE 3 Perturbation of the S4-S5 linker impedes pore-induced stabilization of the activated voltage sensor. (*A* and *B*) Plot of mean $\tau_{fast}$ component of deactivating current ($\tau_f$ deactivation) and the mean weighted $\tau$ of the off-gating current ($\tau_w$ $I_{g,off}$) as a function of increasing depolarization duration at +60 mV, respectively. Data were fitted to a single exponential function (*A*, $n = 6$; *B*, $n = 5$).

## Characterization of mode-shift behavior in hERG channels

The above data suggest that opening of the hERG channel intracellular pore gate and a slower relaxation process stabilize the voltage sensor in its activated state. This process would be expected to alter the energetic landscape experienced by the voltage sensor during its return upon repolarization. Indeed, what has been called mode-shift behavior of hERG channels has been documented in a number of studies (2,10,11,13). These studies present, however, differing reports of the extent of mode-shift and the effects of, for example, deletion of the N-terminus. To try to reconcile these observations, we sought to characterize and correlate mode-shift behavior of the pore gate and the voltage sensing domain, taking particular care in our attempts to make measurements as close to steady-state conditions as possible.

Mode-shift in hERG channels is prominently displayed when activation and deactivation steps of physiological duration are applied, such as in Fig. 4 *A*. These data demonstrate a profound apparent mode-shift with the voltage-dependence of activation and deactivation separated by ~65 mV on the voltage axis. We sought to characterize the mode-shift behavior of hERG channels and the effect of mutations to better understand how open channel transitions stabilize the activated voltage sensor. Understanding that the unusually slow activation and deactivation gating kinetics of hERG channels may influence the measurement of the mode-shift, we first set out to measure the "true" mode-shift from steady-state measurements, because this has not been done before. The data in Fig. 4, *B* and *C*, show that the large separation of activation and deactivation in Fig. 4 *A* derives largely from the non-steady-state measurement of the intrinsically slow kinetics of these two processes and that measurement of steady-state activation and deactivation, and consequently "true" mode-shift, in hERG channels requires long step durations. Fig. 4 *B* shows the dependence of the activation-voltage relationship on the duration of the depolarizing voltage step. Depolarizing steps of 8 s or more are required to measure steady-state voltage-dependence of activation ($-32.8 \pm 0.3$ mV, $n = 6$), as has been described in Cheng et al. (27) and Viloria et al. (32). Fig. 4 *C* shows that slow hERG channel deactivation also influences measurement of the $V_{1/2}$ of the voltage-dependence of deactivation. Using a 15 s depolarizing step to fully activate channels, the repolarization of voltage steps to different voltages was applied for different durations. The data show that allowing slow deactivation to reach steady state shifted the voltage-dependence of deactivation to more depolarized potentials (see Table 1 for Boltzmann fit parameters). Fig. 4 *D* plots the dependence of the $V_{1/2}$ of the activation- and deactivation-voltage relationships on step duration. These data demonstrate that recording activation and deactivation at steady state greatly alters the measured report of the mode-shift of the WT channel. Extrapolated single exponential fits of the data approximate that the "true" mode-shift in hERG channels is ~15 mV. Double exponential fits yielded a value of ~7 mV, and the better fit suggests that although the single exponential provides a reasonable estimate, longer durations may be required to determine the exact value of the "true" mode-shift. This approximated mode-shift represents the separation of the voltage-dependencies of activation and deactivation that is not dependent upon the step duration. These data highlight the influence of voltage step duration on the reporting of the voltage-dependence of both activation and deactivation gating in hERG channels, and consequently, the extent of mode-shift.

Fig. 5 shows measurement of the "true" mode-shift of gating charge movement in hERG channels. Fig. 5 *A* shows on-gating charge-voltage relationships constructed from recordings of the off-gating current during repolarization from depolarizing steps of different duration. The $V_{1/2}$ of steady-state on-gating charge movement was $-42.9 \pm 1.3$ mV ($n = 3$). The dependence of the $V_{1/2}$ of the off-gating charge movement on step duration is shown in Fig. 5 *B* and is summarized in Fig. 5 *C* (see Table 1 for Boltzmann fit

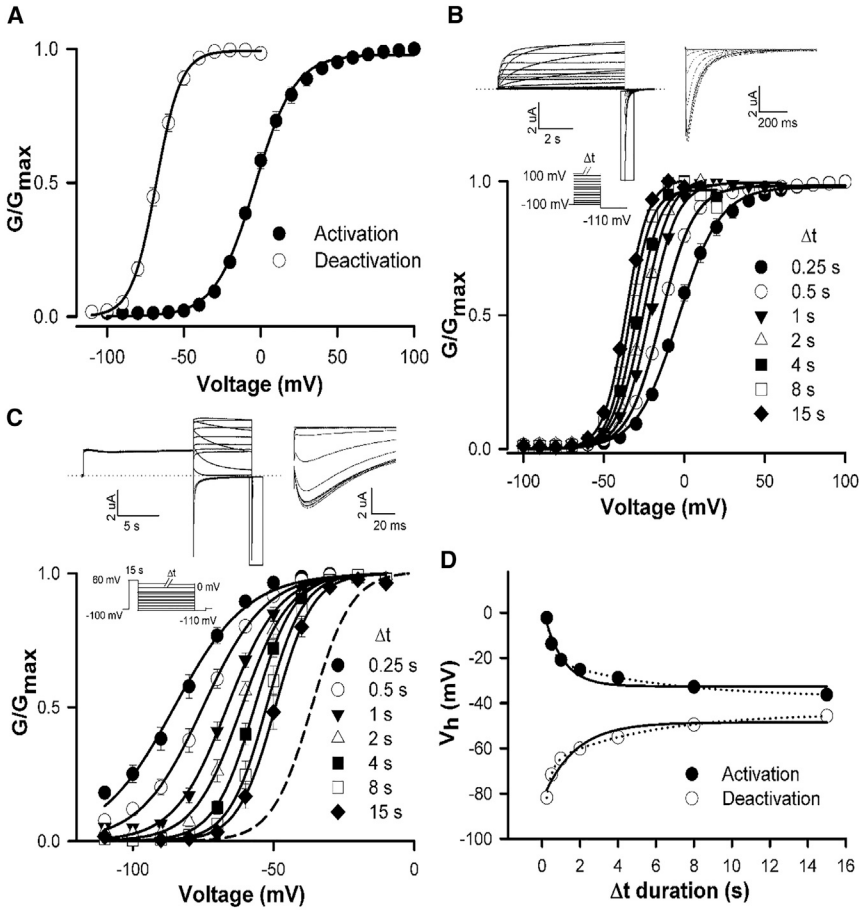


FIGURE 4 Measurement of "true" mode-shift in WT hERG channels. (*A*) Plot of mean WT hERG GV relationships for activation and deactivation measured with voltage steps of physiological duration. For activation, oocytes were held at −100 mV and subjected to 250 ms depolarizing steps to +100 mV in 10 mV increments followed by a repolarizing voltage step to −110 mV. For deactivation, oocytes were held at −100 mV and subjected to a 250 ms depolarizing step +60 mV and then to 750 ms voltage steps to −110 mV in 10 mV increments followed by a repolarizing voltage step to −110 mV. Data were fitted with a Boltzmann function. (*B* and *C*) (*Top*) Typical WT ionic current traces recorded during protocols to measure activation (*B*) and deactivation (*C*) at steady state. For activation, oocytes were held at −100 mV and subjected to 8 s voltage steps to +60 mV in 10 mV increments, followed by a 3.5 s repolarizing step to −110 mV. For deactivation, oocytes were held at −100 mV and subjected to a 15 s depolarizing step +60 mV followed by 8 s repolarizing voltage steps from −110 mV to +40 mV in 10 mV increments and then a 100 ms repolarizing step to −110 mV. (*Inset*) Currents on an expanded timescale to highlight the peak tail current. (*Bottom*) Plot of WT hERG mean GV relationships for activation (*B*) and deactivation (*C*) constructed from normalized peak tail currents ($n = 6$) following the different prepulse durations. For both activation and deactivation, the protocols were repeated in the same cell with different $\Delta t$ durations and the mean $V_h$ and $k$ values were obtained by fitting each data set to a Boltzmann function (see Table 1). These data demonstrate the approach toward steady-state activation and deactivation GV relations with increasing $\Delta t$ duration. The dashed line in (*C*) represents the steady-state activation GV relation of WT hERG shown in (*B*). (*D*) Relationship between $V_h$ of activation and deactivation with the $\Delta t$ duration, as determined from the data presented in (*B*) and (*C*). Data are fitted with extrapolated single (*solid line*) or double (*dotted line*) exponential functions. Single exponential extrapolated steady-state values for activation and deactivation $V_h$ were −33 and −48 mV. The equivalent values for double exponential fits were −38 and −45 mV, respectively.

parameters). Extrapolated single and double exponential fits of the dependence of the $V_{1/2}$ of on- and off-gating charge on step duration show that the approximated "true" voltage sensor mode-shift is ~40 mV. This is much greater than the ionic current mode-shift (~15 mV). Fig. 5 *D* demonstrates this by directly comparing the steady-state voltage dependence of ionic current activation and deactivation on the same axis as the steady-state voltage-dependence of on- and off-gating charge movement. The plot shows that upon repolarization the hERG channel pore closes at voltages that do not return significant charge. For example, at −50 mV, the open probability of the pore is reduced by ~80% when only roughly 20% of the charge returns. These data show that, upon

**TABLE 1 Activation and Deactivation GV, and $I_{g,\,on}$ and $I_{g,\,off}$ QV Boltzmann Fit Parameters for WT hERG Channels with Different Depolarizing Step Durations ($\Delta t$)**

| | Activation GV | | | Deactivation GV | | | $I_{g,\,on}$ QV | | | $I_{g,\,off}$ QV | | |
|---|---|---|---|---|---|---|---|---|---|---|---|---|
| $\Delta t$ (s) | $V_h$ (mV) | $k$ (mV) | $n$ | $V_h$ (mV) | $k$ (mV) | $n$ | $V_h$ (mV) | $k$ (mV) | $n$ | $V_h$ (mV) | $k$ (mV) | $n$ |
| 0.1 | — | — | — | — | — | — | −9.5 ± 2.3 | 15.5 ± 0.5 | 5 | −100.8 ± 5.0 | 15.5 ± 0.7 | 6 |
| 0.25 | −2.2 ± 1.6 | 13.5 ± 2.3 | 6 | −81.8± 2.0 | 11.8 ± 0.4 | 6 | −19.9 ± 1.3 | 14.1 ± 0.8 | 7 | −95.9 ± 2.7 | 15.2 ± 0.5 | 6 |
| 0.5 | −13.7 ± 0.8 | 10.1 ± 1.7 | 6 | −71.6 ± 0.8 | 9.8 ± 0.6 | 6 | −25.5 ± 1.4 | 14.7 ± 1.4 | 7 | −92.8 ± 2.2 | 12.3 ± 0.7 | 7 |
| 1 | −20.8 ± 0.2 | 8.8 ± 1.3 | 6 | −64.6 ± 0.4 | 7.7 ± 0.5 | 6 | −30.9 ± 1.4 | 11.8 ± 0.5 | 7 | −86.2 ± 2.8 | 12.7 ± 1.0 | 7 |
| 2 | −25.3 ± 0.5 | 8.1 ± 1.2 | 6 | −60.1 ± 0.6 | 6.6 ± 0.4 | 6 | −32.3 ± 1.4 | 12.0 ± 1.3 | 6 | −81.2 ± 2.7 | 12.0 ± 1.4 | 4 |
| 4 | −28.8 ± 0.8 | 7.7 ± 1.2 | 6 | −55.0 ± 0.4 | 6.2 ± 0.4 | 6 | −40.0 ± 1.6 | 7.6 ± 0.9 | 4 | −77.5 ± 2.3 | 10.1 ± 1.2 | 7 |
| 8 | −32.8 ± 0.3 | 7.1 ± 1.2 | 6 | −49.5 ± 0.5 | 5.7 ± 0.4 | 6 | −42.9 ± 1.4 | 8.4 ± 0.4 | 3 | — | — | — |
| 15 | −36.3 ± 0.4 | 6.8 ± 1.1 | 6 | −45.7 ± 0.4 | 5.5 ± 0.4 | 6 | — | — | — | — | — | — |

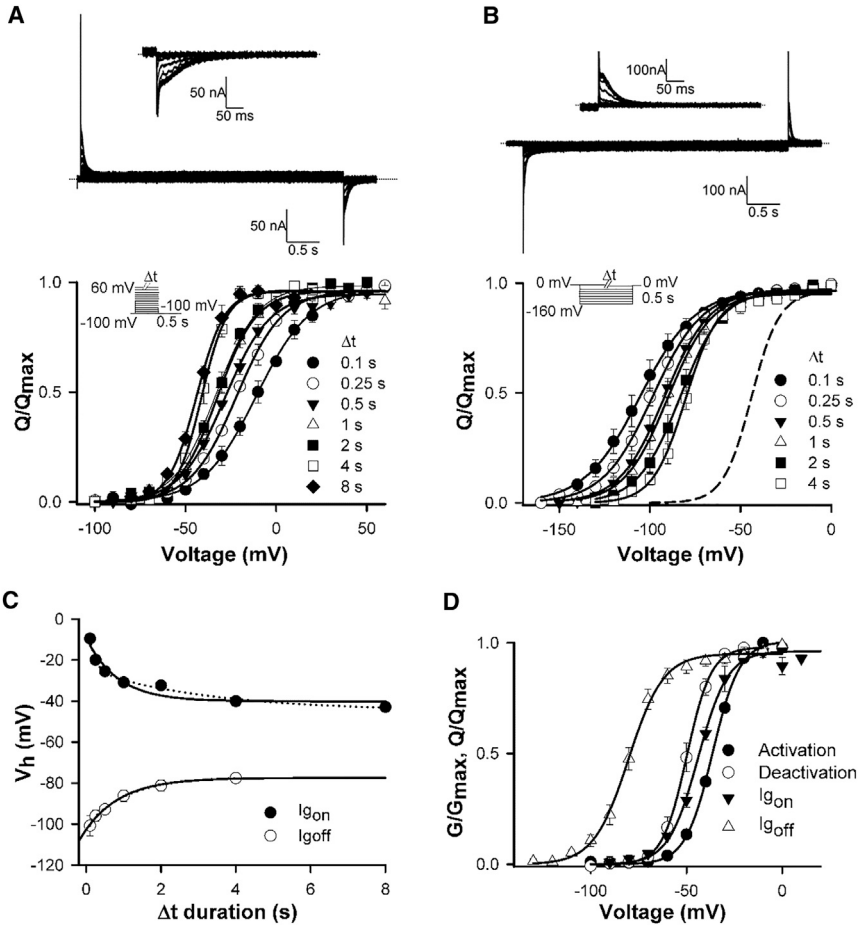


FIGURE 5 Uncoupling of the voltage sensor from the pore during deactivation. (*A* and *B*) (*Top*) Typical WT on-gating (*A*) and off-gating (*B*) currents. For on-gating currents, oocytes were held at −100 mV and subjected to 4 s voltage steps to +60 mV in 10 mV increments. Gating charge moved was determined from the integral of the off-gating current measured during the 500 ms step back to −100 mV. (*A*, *inset*) Off-gating currents are enlarged for clarity. For off-gating currents, oocytes were held at 0 mV and subjected to 4 s repolarizing steps to −160 mV in 10 mV increments. Gating charge moved was determined from the integral of the on-gating currents measured during the 500 ms step back to 0 mV. (*B*, *inset*), On-gating currents are enlarged for clarity. (*Bottom*) Plots of mean WT hERG QV relationships for on-gating (*A*) and off-gating (*B*) measured with varying depolarizing or repolarizing pulse durations ($\Delta t$). For both on- and off-gating, mean $V_h$ and $k$ values were obtained by fitting to a Boltzmann function (see Table 1). The dashed line in (*B*) represents the steady-state on-gating QV relation shown in (*A*). (*C*) Relationship between $V_h$ of on- and off-gating with $\Delta t$ duration, as determined from (*A*) and (*B*). Data are fitted with extrapolated single (*solid line*) or double (*dotted line*) exponential functions. Single exponential extrapolated steady-state values for on- and off-gating $V_h$ were −40 and −77 mV. The equivalent values for double exponential fits were −45 and −77 mV, respectively. (*D*) Summary of the steady-state GV and QV relations highlighting the uncoupling of voltage sensor return from pore closure.

repolarization, pore closing is more energetically favorable than the return of the gating charges.

## The role of the N-terminus in stabilizing the activated voltage sensor and mode-shift

The N-terminus is well known to modify hERG deactivation gating by slowing pore closure; however, the underlying mechanism is unclear. Some insight came from two recent studies (10,13) that investigated the role of the N-terminus in mode-shift behavior; however, the reported effect of N-terminal deletion on mode-shift differed. We reasoned that these findings might be reconciled based on our findings above that the apparent mode-shift is influenced by the recording step duration. To test this, we measured mode-shift behavior in channels lacking the distal N-terminus (Δ2–135) with step durations that were long enough to record activation and deactivation at steady state. We also measured the effect of N-terminal deletion on stabilization of the activated voltage sensor.

Fig. 6, *A–C*, demonstrates the measurement of "true" mode-shift in hERG Δ2–135 channels. These data show that, as in the case of the WT channel, the apparent mode-shift is highly dependent upon the voltage step durations used for recording both activation and deactivation (see Table S1 for Boltzmann fit parameters). The "true" mode-shift in hERG Δ2–135 channels is ~6 mV, which is similar to the approximated value in WT channels. These data suggest that the N-terminal domain does not play a significant role in mode-shift behavior. Consistent with this, Fig. 6, *D–G*, shows the effect of depolarizing step duration on ionic current deactivation and gating charge return in hERG Δ2–135 channels. The data show that both channel deactivation and gating charge return were faster in hERG Δ2–135 channels compared with WT hERG channels. However, most interestingly, both measures were slowed by increased depolarization step durations in a biphasic manner. Channel deactivation was slowed with $\tau_{fast}$ and $\tau_{slow}$ values of 59.8 ± 4.5 ms (relative contribution 0.37 ± 0.02) and 2.6 ± 0.6 s (relative contribution 0.63 ± 0.02), respectively ($n = 5$). Gating charge return was slowed with $\tau_{fast}$ and $\tau_{slow}$ values of 12.7 ± 1.4 ms (relative contribution 0.26 ± 0.02) and 4.3 ± 1.5 s (relative contribution 0.73 ± 0.02), respectively ($n = 12$). These data demonstrate that, as in the case of WT channels, depolarization slowed voltage sensor return in a biphasic manner with a fast phase of slowing of both charge return and channel deactivation that occurred over a similar time-frame to channel opening

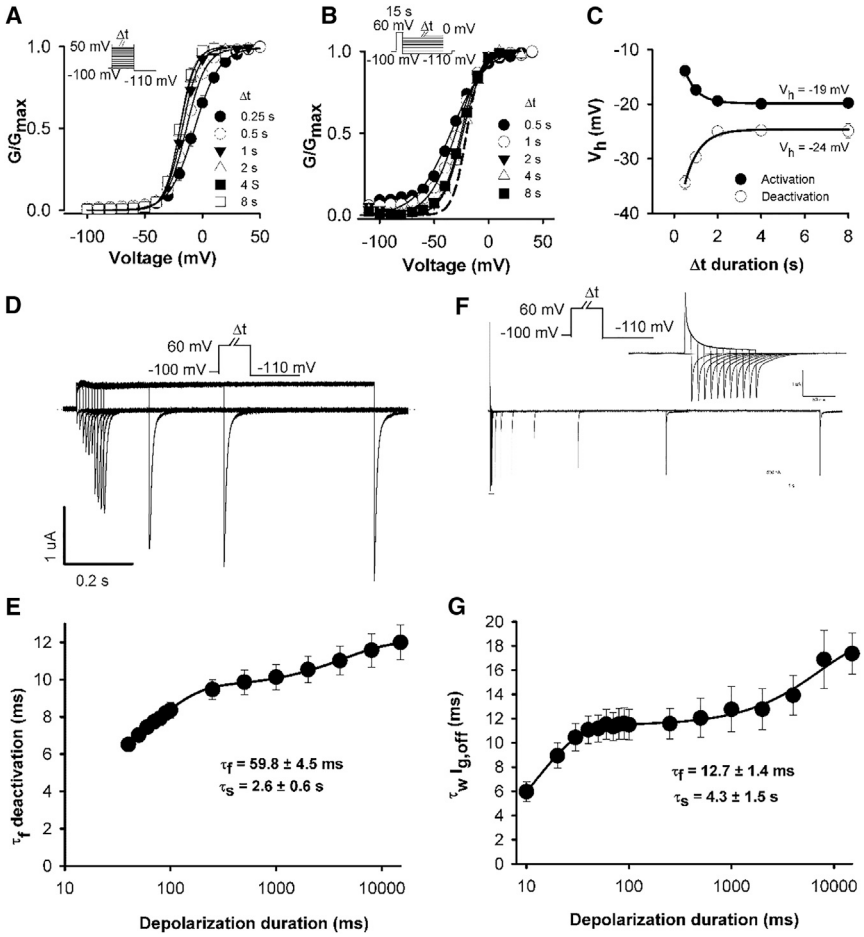


FIGURE 6 Effect of deletion of the distal N-terminus on voltage sensor stabilization. (*A* and *B*) Plot of mean hERG Δ2–135 GV relationships for activation (*A*) and deactivation (*B*) constructed from normalized peak tail currents with different prepulse durations ($n = 5$). Activation and deactivation were recorded in the same cells with different $\Delta t$ durations and the mean $V_h$ and $k$ values were obtained by fitting each data set to a Boltzmann function (see Table S1). These data demonstrate the approach toward steady-state activation and deactivation GV relations with increasing $\Delta t$ duration. (*Dashed line* in *B*) Steady-state activation GV relation of hERG Δ2–135 in (*A*). (*C*) Relationship between $V_h$ of activation and deactivation with the $\Delta t$ duration, as determined from the data in (*A*) and (*B*). Data are fitted with an extrapolated exponential function. (*D* and *F*) Typical ionic (*D*) and gating (*F*) current traces from hERG Δ2–135 channels recorded in response to the protocol shown in which the depolarizing test pulse duration was varied. (*Inset* in *F*) Currents on an expanded timescale to highlight the off-gating current decay. (*E* and *G*) Plot of the mean $\tau_{fast}$ component of deactivating ionic current ($\tau_f$ deactivation) and the mean weighted $\tau$ of the off-gating current ($\tau_w I_{g,off}$) as a function of increasing depolarization duration at +60 mV, respectively. Data were fitted to a double exponential function.

(hERG Δ2–135 activation $\tau = 73 \pm 7$ ms at +60 mV, $n = 6$). These data show that while deletion of the N-terminus accelerates the kinetics of voltage sensor return, both open pore- and relaxation-induced stabilization of the voltage sensor are preserved in hERG channels lacking the N-terminus. These data show that voltage sensor stabilization in response to depolarization is preserved in hERG channels lacking the N-terminus.

## Accelerated deactivation kinetics result in an apparent reduction in mode-shift

The data in Figs. 4 and 5 show that incomplete measurement of channel deactivation and gating charge return in WT hERG channels produces an apparent mode-shift behavior that does not reflect "true" mode-shift behavior. We reasoned that fast deactivation in channels lacking the N-terminus allows more complete measurement of deactivation and creates an apparent loss of mode-shift when compared with WT channels in which deactivation is slower and requires voltage steps of 8 s or more to reach steady-state (Fig. 4). Consistent with this, when standard voltage step durations were used, measurements of the voltage-dependence of activation and deactivation in WT channels resulted in an overestimation of the mode-shift (Table 2). In numerous mutant channels, fast deactivation gating meant that the voltage-dependence of deactivation was closer to steady state and resulted in an apparent reduction in mode-shift behavior. This was the case for mutations made at sites throughout the hERG channel, such as R4D and R5E in the N-terminus, D456A in S2, E480R in the S2-S3 linker, D509A in S3, R537K, R541G, Y542G, and E544G in the S4-S5 linker. Table 2 shows that in each of these cases, the apparent reduction in mode-shift behavior could be explained by accelerated kinetics of channel deactivation.

## S3-S4 linker length does not influence stabilization of activated hERG channel states

Our data in hERG channels are consistent with previous studies in other Kv channels in that they suggest that a slow voltage sensor stabilization or relaxation occurs due to prolonged depolarization. Previous studies suggest that this property is intrinsic to the voltage sensor and one study showed that the S3-S4 linker plays a role in stabilizing the activated configuration of the voltage sensor in response to prolonged depolarization in *Shaker* channels (22).

**TABLE 2 Correlation of Apparent Mode-shift with Deactivation Kinetics**

| | Activation GV | | | Deactivation GV | | | Mode-shift | | Deactivation $\tau$—$\tau_f$ (ms) | |
|---|---|---|---|---|---|---|---|---|---|---|
| | $V_h$ (mV) | $k$ (mV) | $n$ | $V_h$ (mV) | $k$ (mV) | $n$ | $V_h$ (mV) | $n$ | −110 mV | $n$ |
| WT | −22.8 ± 1.1 | 10.8 ± 0.7 | 13 | −54.2 ± 1.6 | 7.8 ± 0.4 | 13 | −31.4 ± 2.1 | 13 | 94.8 ± 9.3 | 8 |
| R4D | −14.9 ± 1.0 | 9.2 ± 0.3 | 5 | −22.8 ± 1.1 | 7.5 ± 0.8 | 5 | −7.8 ± 1.6 | 5 | 27.5 ± 2.5 | 4 |
| R5E | −17.6 ± 2.0 | 9.6 ± 0.3 | 5 | −30.1 ± 1.4 | 7.8 ± 0.5 | 5 | −12.5 ± 1.0 | 5 | 47.9 ± 5.7 | 4 |
| D456A | −1.0 ± 1.2 | 7.5 ± 0.4 | 5 | −7.0 ± 1.0 | 7.5 ± 0.6 | 5 | −6.0 ± 0.9 | 5 | 35.8 ± 2.5 | 5 |
| E480R | −2.8 ± 0.6 | 10.0 ± 0.2 | 5 | −14.0 ± 1.7 | 8.4 ± 0.5 | 5 | −11.8 ± 2.3 | 5 | 47.0 ± 3.5 | 5 |
| D509A | 14.3 ± 1.5 | 11.0 ± 0.2 | 4 | 8.3 ± 0.7 | 9.9 ± 0.7 | 4 | −6.0 ± 1.4 | 4 | 22.0 ± 2.0 | 4 |
| R537K | −8.6 ± 3.7 | 8.0 ± 0.3 | 6 | −9.8 ± 3.7 | 8.3 ± 0.4 | 6 | −1.2 ± 0.7 | 6 | 55.2 ± 2.3 | 5 |
| R541G | −35.2 ± 1.5 | 13.2 ± 0.5 | 5 | −41.7 ± 1.2 | 11.7 ± 0.4 | 5 | −6.5 ± 0.6 | 5 | 42.8 ± 1.6 | 7 |
| Y542G | −4.9 ± 2.1 | 14.8 ± 1.0 | 5 | −14.9 ± 1.4 | 11.1 ± 0.7 | 5 | −10.0 ± 1.6 | 5 | 12.9 ± 0.5 | 9 |
| E544G | −22.4 ± 0.5 | 8.5 ± 0.1 | 7 | −25.3 ± 0.8 | 7.5 ± 0.2 | 7 | −2.9 ± 0.6 | 7 | 18.9 ± 0.6 | 5 |

Activation GV relations were collected from oocytes held at −80 mV and subjected to 2 s depolarizing steps to +50 mV in 10 mV increments followed by a 2 s step to −110 mV. Deactivation GV relations were collected from oocytes held at −80 mV and subjected to a 500 ms depolarizing step +60 mV followed by 8 s steps from –110 mV to +40 mV in 10 mV increments followed by a repolarizing step to −110 mV. Boltzmann fits were used to obtain the $V_h$ and $k$ values. Deactivation $\tau$ was obtained by fitting the deactivation tail current decay with a double exponential function. The value $\tau_{fast}$ is reported, because current decay at −110 mV was dominated (>85%) by the fast component.

This study predicted greater voltage sensor stabilization in channels with shorter S3-S4 linker lengths, although linker composition, such as the negative charge cluster, EEED, were also suggested to play a role. To investigate the role of the relatively short hERG S3-S4 linker and its composition in the stabilization of the activated state, mode-shift was measured in WT hERG channels and compared with mutant channels in which the short, 9-residue, S3-S4 linker was replaced with the longer, 31-residue, linker from *Shaker* channels (hERG/Sh), or in which the nine residues of the native hERG S3-S4 linker were replaced with glycine amino acids (hERG/9G; Fig. 7 *A*). Fig. 7 *B* shows mean activation- and deactivation-voltage relationships for each of these constructs (see Table S2 for Boltzmann fit parameters). These experiments were designed with non-steady-state pulse durations so that a loss of mode-shift because of linker perturbation would be detectable compared to the mode-shift recorded in WT channels. The mean mode-shift that we recorded was –31.3 ± 2.0 mV ($n$ = 5), –34.5 ± 1.2 mV ($n$ = 5), and −28.8 ± 1.1 ($n$ = 4) mV in WT, hERG/Sh, and hERG/9G channels, respectively. Given this lack of effect of the S3-S4 linker, a putative role of the S1-S2 linker in mediating voltage sensor stabilization was also investigated. Truncation of the majority of the S1-S2 linker produced nonfunctional channels, but channels in which a negative charge cluster, ETEE, in the S1-S2 linker were neutralized to glutamine residues (Fig. 7 *C*) were functional. The mean mode-shift in ETEE/QQQQ mutant hERG channels (Fig. 7 *D*) was –24.5 ± 2.9 mV ($n$ = 5), which was not significantly different from that in WT channels –24.1 ± 4.5 mV ($n$ = 5). These data suggest that the extracellular S3-S4 linker does not play a role in stabilizing the activated hERG voltage sensor configuration as has been shown in other channel types, indicating that other regions within the hERG voltage sensing unit that are yet to be identified may contribute to the mode-shift phenomenon.

## DISCUSSION

This study provides, to our knowledge, novel insight into the link between activation and deactivation gating in hERG

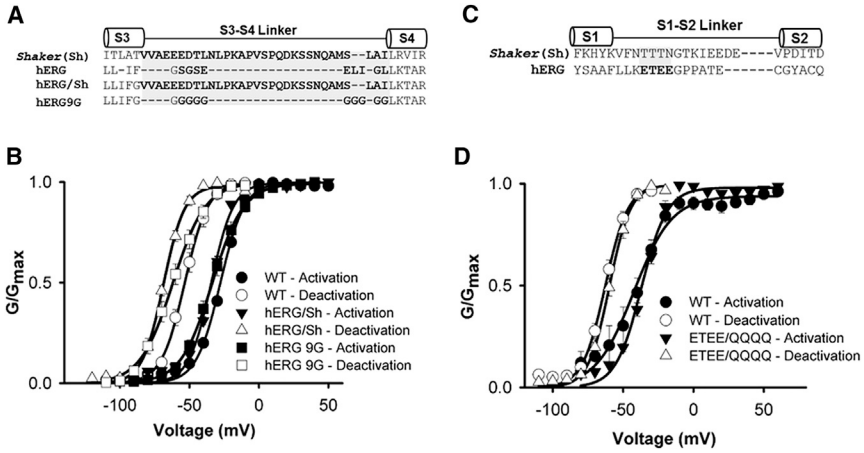


FIGURE 7 Mode-shift in hERG channels is not dependent upon S3-S4 or S1-S2 linker structure. (*A* and *C*) Sequence alignment of the S3-S4 (*A*) and S1-S2 (*C*) linker in *Shaker* and hERG channels. (*B* and *D*) Plots of mean GV relationships for hERG WT, hERG/Sh, and hERG 9G (*B*) and hERG ETEE/QQQQ (*D*) activation and deactivation constructed from normalized peak tail currents. Mean $V_h$ and $k$ values were obtained by fitting each data set to a Boltzmann function (Table S2).

channels. The data show that the activated voltage sensor configuration is stabilized by depolarization via two separable mechanisms, one that derives from the open pore gate and another from within the voltage sensing unit itself. We have characterized the mode-shift behavior that this produces by measuring activation and deactivation, as well as on- and off-gating currents, at steady state and this shows that the pore gate in hERG channels can close while the voltage sensors remain in their activated position. Lastly, we demonstrate that coupling between the pore gate and voltage sensor during deactivation is impeded by perturbation of the S4-S5 linker, but remains intact in Δ2–135 channels.

## Prepulse-dependent slowing of hERG deactivation

Biphasic slowing of deactivation in response to increasing depolarizing step duration, such as that which we characterize in hERG channels in Figs. 1 and 2, has been observed in *Shaker* and Kv1.2 channels (19–21). In these channels, the faster phase of deactivation slowing was kinetically associated with pore opening, which was interpreted by the authors to suggest that rearrangements of the pore gate during activation, limit pore closure. The slower phase of deactivation slowing occurred with depolarization durations that exceeded the time course of channel activation. Both components of the slowing of channel deactivation correlated well with measurements of gating charge return, leading the authors to conclude that the slowed deactivation emanated from events intrinsic to the voltage sensor that were influenced by the opening of the pore. Our data in hERG channels are consistent with this interpretation and suggest that both mechanisms are conserved features of gating in hERG channels. Firstly, the time course of channel opening and the faster component of deactivation slowing with increasing depolarization duration are reasonably well correlated despite the fact that activation of the pore gate in hERG channels is ~10-fold slower than in *Shaker* and Kv1.2 channels. This is consistent with a role for pore opening in the retardation of closing. Interestingly, the $\tau$ of the fast phase of slowing of gating charge return (34 ms) was faster than that of deactivation gating (93 ms) in hERG channels. This suggests that the faster slowing of charge return may occur in response to events earlier in the activation pathway (35–40% of channels are open after a 35 ms at +60 mV (5)), while the faster slowing of pore closure during deactivation appears to occur in response to events later in the activation pathway when channels are fully activated.

It is interesting that the time course of the slower component of voltage sensor slowing was similar in hERG channels (~2.5 s) to that reported (~1.1 s) in *Shaker* and Kv1.2 channels (19) despite the fact that inactivation properties are quite distinct in the different channels. The delayed phase was attributed to a relaxation process whereby the voltage sensor assumes a more stable lower energy state in response to prolonged depolarization (19,20). Several lines of evidence suggest that relaxation is an intrinsic voltage sensor property that is distinct from inactivation mechanics. For example, relaxation is preserved in a voltage sensor protein that lacks a pore domain (Ci-VSP (21)) and therefore the effector of inactivation (19). However, others have suggested that delayed charge return may result from voltage-independent steps that are a prelude to, or associated with, the inactivation process (25). The similar kinetics of the slow process despite stark differences in inactivation properties (*Shaker* and Kv1.2 inactivation occurs on the timescale of seconds and is voltage-independent, whereas hERG inactivation is strongly voltage-dependent and occurs with a $\tau$ of a few milliseconds at depolarized potentials) leads us to suggest that the relaxation process is unrelated to inactivation in hERG channels.

## S4-S5 linker coupling during deactivation

Several studies have suggested that the S4-S5 linker that connects the voltage sensor domain with the pore domain is involved in the coupling of charge movement with pore gate opening (1–5,33). However, recent evidence suggests that the mechanism of coupling in hERG channels may be different from that in other *Shaker*-like Kv channels. The recent cryo-EM structure of the *eag* channel reveals that the S4-S5 linker in *eag*, and related channels such as hERG, may be too short to function as a mechanical lever that influences the pore gate (6). This idea is supported by the observation that activation gating is not strongly influenced in channels in which the physical connection between the S4-S5 linker and the pore domain is disrupted (7).

We have previously shown that mutation of G546, to any other residue that reduced $\alpha$-helical propensity, shifted the voltage-dependence of activation ~50 mV to more hyperpolarized potentials (5). This suggested to us that G546 is an important site that mediates the open-closed equilibria in hERG channels. Here, we have used mutation of G546 in the S4-S5 linker as a perturbation tool to investigate the role of the S4-S5 linker in deactivation gating. We were further driven to investigate the S4-S5 linker by the observation that disruption of the physical connection between the voltage sensor and pore domains, while not influencing activation greatly, impacted deactivation gating significantly (7). Furthermore, evidence from *Shaker* channels suggests that the S4-S5 linker couples the pore and voltage sensor during deactivation based on the observation that specific interactions between residues in the S4-S5 linker and the pore control mode-shift behavior (24).

Fig. 3 shows that the G546L mutation appeared to specifically impede the faster component of voltage sensor stabilization that is associated with opening reconfigurations of the pore gate without attenuating the slower relaxation phase, because there is no obvious phase of slowing of charge return

and deactivation gating that occurs on the same timescale as pore opening. This suggests that S4-S5 linker perturbation interferes with pore-to-voltage sensor coupling during deactivation. An alternate possibility is that the fast phase of slowing is preserved in G546L channels, but that it occurs in response to much shorter duration prepulse steps than tested here. However, if this were the case, the proportion of this phase would be dramatically reduced compared with WT channels, and would still be temporally dissociated from activation of the pore gate of the channel. Thus, we interpret the data to indicate that the S4-S5 linker perturbation interferes with the influence of the pore gate on the stability of the voltage sensor and supports a role for the short helical connector in communicating reconfigurations of the open pore to the voltage sensor. It is also possible that reduced flexibility of the linker in the G546L mutant channel limits the configurations of the pore gate that are associated with increased stability of the activated voltage sensor, but our data cannot distinguish between these mechanisms. In either case, the data from the mutant channel suggest that in WT channels the pore drives one aspect of voltage sensor return, and a separable relaxation mechanism drives a slower stabilization of the activated voltage sensor. This latter mechanism appears therefore to originate from upstream of the S4-S5 linker, further supporting the conclusion that it originates from within the voltage sensor itself. Taken together, these data suggest that voltage sensor return and closing of hERG channels is dually regulated by the pore gate upon opening, and by intrinsic voltage sensor rearrangements. These processes are predicted to dictate slow deactivation in hERG channels enabling the provision of a resurgent cardiac repolarizing current. Interestingly, a recent study showed that the drug retigabine preferentially stabilized Kv7.2/Kv7.3 channels in the relaxed state (34), suggesting that selective targeting of the relaxed state in these channels, or hERG channels for that matter, may offer therapeutic potential.

The influence of S4-S5 linker perturbation on communication between the pore and voltage sensor during deactivation described in this study is significant given the recent structural description of *eag* channels (6). Based upon the short length of the S4-S5 linker, the authors interpreted these structures to demonstrate that the mechanism of voltage-dependence in the *eag* family of channels (which includes hERG) may differ from the classical S4-S5 linker-mediated electromechanical coupling described in *Shaker*-like channels. An alternate mechanism involving integration of the PAS domain and CNBHD by calmodulin was proposed to gate the *eag* intracellular pore independent of voltage changes. Voltage sensor motions during activation were predicted to alter interactions of the S4-S5 linker with S6, which then positions S4 to interact with the C-linker region and open the pore. Our data are consistent with this model of voltage sensing. Firstly, Fig. 5 provides functional evidence supporting the structural observation that the pore gate can close with voltage sensors in the activated position. Secondly, Fig. 3 shows that the S4-S5 linker influences the communication of pore gate reconfigurations upon opening to the activated voltage sensor. This is consistent with the observed interaction between the S4-S5 linker and the lower portion of S6 when the voltage sensors are in the activated position in the *eag* structure (6).

## Characterization of mode-shift behavior in hERG channels

Stabilization of activated states during depolarization results in delayed charge return and channel deactivation, which has been described as mode-shift behavior. Mode-shift has been reported in hERG channels (2,10,11,13), but is dependent on recording conditions. This makes comparison of the effects of mutations challenging. In Figs. 4 and 5, we characterized the mode-shift of ionic current and of charge movement in hERG channels by measuring steady-state activation and deactivation, and on- and off-gating current, respectively. These data show that the "true" mode-shift of the pore gate is ~15 mV while that of the voltage sensor is ~40 mV. From these data, we draw two conclusions. Firstly, the reporting of mode-shift is highly dependent upon the kinetics of activation and deactivation and the step durations used to record on-gating/activation and off-gating/deactivation. We observed an apparent loss of mode-shift in many mutant channels (Table 2) that could be accounted for by faster deactivation kinetics than observed in WT channels. Secondly, mode-shift of the voltage sensor is significantly greater than that of the pore gate. This observation demonstrates that voltage sensor return is less energetically favorable than pore closure upon repolarization and demonstrates the important role for voltage sensor relaxation is stabilizing the hERG activated voltage sensor and limiting its return. This finding is consistent with a previous observation of the dissociation between voltage sensor return and pore closure caused by a pharmacological activator compound (29). Furthermore, our data also provide supporting functional evidence for the recent cryo-EM structural prediction of the related *eag* channel, which captures the channel in a state in which the pore gate is closed, but the voltage sensor is in the activated configuration (6). We may also interpret the data in Fig. 5 *D* to demonstrate that not all charges must return upon repolarization for the pore gate of hERG channels to close. hERG channel gating schemes include independent voltage sensor transitions (11), which supports the idea that the pore may close is response to return of only a portion of gating charge. Indeed, a role for individual voltage sensor subunits within the channel tetramer has been documented (35).

## The role of the N-terminus in coupling during mode-shift

Deletion of the N-terminus of hERG channels accelerates deactivation kinetics, suggesting that the cytoplasmic

domain stabilizes the open state of the pore gate (10,13,36–39). The desire to understand this fundamental mechanism is underscored by the observation that inherited mutations, such as R56Q in the N-terminus, accelerate deactivation and predispose to Long QT syndrome and sudden cardiac death (40). Two studies recently reported the effects of deletion of the N-terminus on mode-shift behavior to address this question, but the reported effects differed (10,13). Here, using steady-state measurements of activation and deactivation, we demonstrate that mode-shift of the pore gate in Δ2–135 hERG channels is similar to that in WT channels. Moreover, coupling between the pore gate and voltage sensor appears intact, because voltage sensor return was slowed by channel opening in a similar biphasic manner to that observed in WT channels. These data suggest that the N-terminus does not abolish the stabilizing influence of the pore on the voltage sensor. It is interesting, however, that the fast phase of slowing of gating charge return and pore gate closure were accelerated in Δ2–135 channels compared with WT channels ($P < 0.05$). This implies that perturbation of the N-terminus accelerates the kinetics of open pore stabilization of the activated voltage sensor. A possible interpretation of this finding is that deactivation in WT channels is limited by transitions occurring as the pore opens that stabilize the open pore and the activated voltage sensor. Truncation of the N-terminus apparently accelerates these transitions and this could underlie the faster deactivation kinetics in Δ2–135 channels. Further studies are required to clarify this influence of the N-terminus on the stability of the activated voltage sensor.

## SUPPORTING MATERIAL

Two figures and two tables are available at http://www.biophysj.org/biophysj/supplemental/S0006-3495(16)34325-9.

## AUTHOR CONTRIBUTIONS

S.T., C.M.H., Y.P.S., Y.M.C., and T.W.C. conceived the project and wrote the article; and S.T., C.M.H., Y.P.S., V.S., J.Y., and Y.M.C. performed experiments and data analysis.

## ACKNOWLEDGMENTS

The authors thank Ji Qi for excellent technical assistance.

This research was supported by a Heart and Stroke Foundation of British Columbia and Yukon Grant-In-Aid and a Natural Sciences and Engineering Research Council of Canada Discovery Grant held by T.W.C. C.M.H. was supported by a Natural Sciences and Engineering Research Council of Canada Alexander Graham Bell Canada Graduate Scholarship.

## REFERENCES

1. Ferrer, T., J. Rupp, …, M. Tristani-Firouzi. 2006. The S4–S5 linker directly couples voltage sensor movement to the activation gate in the human ether-á-go-go-related gene (hERG) K+ channel. *J. Biol. Chem.* 281:12858–12864.
2. Hull, C. M., S. Sokolov, …, T. W. Claydon. 2014. Regional flexibility in the S4–S5 linker regulates hERG channel closed-state stabilization. *Pflugers Arch.* 466:1911–1919.
3. Sanguinetti, M. C., and Q. P. Xu. 1999. Mutations of the S4-S5 linker alter activation properties of hERG potassium channels expressed in *Xenopus* oocytes. *J. Physiol.* 514:667–675.
4. Tristani-Firouzi, M., J. Chen, and M. C. Sanguinetti. 2002. Interactions between S4-S5 linker and S6 transmembrane domain modulate gating of hERG $K^+$ channels. *J. Biol. Chem.* 277:18994–19000.
5. Van Slyke, A. C., S. Rezazadeh, …, T. W. Claydon. 2010. Mutations within the S4–S5 linker alter voltage sensor constraints in hERG K+ channels. *Biophys. J.* 99:2841–2852.
6. Whicher, J. R., and R. MacKinnon. 2016. Structure of the voltage-gated $K^+$ channel Eag1 reveals an alternative voltage sensing mechanism. *Science.* 353:664–669.
7. Lorinczi, E., J. C. Gomez-Posada, …, L. A. Pardo. 2015. Voltage-dependent gating of KCNH potassium channels lacking a covalent link between voltage-sensing and pore domains. *Nat. Commun.* 6:6672.
8. Bezanilla, F. 1982. Gating charge movements and kinetics of excitable membrane proteins. *Prog. Clin. Biol. Res.* 79:3–16.
9. Bruening-Wright, A., and H. P. Larsson. 2007. Slow conformational changes of the voltage sensor during the mode shift in hyperpolarization-activated cyclic-nucleotide-gated channels. *J. Neurosci.* 27:270–278.
10. Goodchild, S. J., L. C. MacDonald, and D. Fedida. 2015. Sequence of gating charge movement and pore gating in hERG activation and deactivation pathways. *Biophys. J.* 108:1435–1447.
11. Piper, D. R., A. Varghese, …, M. Tristani-Firouzi. 2003. Gating currents associated with intramembrane charge displacement in hERG potassium channels. *Proc. Natl. Acad. Sci. USA.* 100:10534–10539.
12. Shirokov, R., R. Levis, …, E. Rios. 1992. Two classes of gating current from L-type Ca channels in guinea pig ventricular myocytes. *J. Gen. Physiol.* 99:863–895.
13. Tan, P. S., M. D. Perry, …, A. P. Hill. 2012. Voltage-sensing domain mode shift is coupled to the activation gate by the N-terminal tail of hERG channels. *J. Gen. Physiol.* 140:293–306.
14. Bezanilla, F., E. Perozo, …, E. Stefani. 1991. Molecular basis of gating charge immobilization in *Shaker* potassium channels. *Science.* 254:679–683.
15. Choi, K. L., C. Mossman, …, G. Yellen. 1993. The internal quaternary ammonium receptor site of Shaker potassium channels. *Neuron.* 10:533–541.
16. Chen, F. S., D. Steele, and D. Fedida. 1997. Allosteric effects of permeating cations on gating currents during K+ channel deactivation. *J. Gen. Physiol.* 110:87–100.
17. Fedida, D., R. Bouchard, and F. S. Chen. 1996. Slow gating charge immobilization in the human potassium channel Kv1.5 and its prevention by 4-aminopyridine. *J. Physiol.* 494:377–387.
18. Olcese, R., R. Latorre, …, E. Stefani. 1997. Correlation between charge movement and ionic current during slow inactivation in *Shaker* $K^+$ channels. *J. Gen. Physiol.* 110:579–589.
19. Labro, A. J., J. J. Lacroix, …, F. Bezanilla. 2012. Molecular mechanism for depolarization-induced modulation of Kv channel closure. *J. Gen. Physiol.* 140:481–493.
20. Lacroix, J. J., A. J. Labro, and F. Bezanilla. 2011. Properties of deactivation gating currents in *Shaker* channels. *Biophys. J.* 100:L28–L30.
21. Villalba-Galea, C. A., W. Sandtner, …, F. Bezanilla. 2008. S4-based voltage sensors have three major conformations. *Proc. Natl. Acad. Sci. USA.* 105:17600–17607.
22. Priest, M. F., J. J. Lacroix, …, F. Bezanilla. 2013. S3–S4 linker length modulates the relaxed state of a voltage-gated potassium channel. *Biophys. J.* 105:2312–2322.

23. Batulan, Z., G. A. Haddad, and R. Blunck. 2010. An intersubunit interaction between S4–S5 linker and S6 is responsible for the slow off-gating component in Shaker $K^+$ channels. *J. Biol. Chem.* 285:14005–14019.

24. Haddad, G. A., and R. Blunck. 2011. Mode shift of the voltage sensors in *Shaker* $K^+$ channels is caused by energetic coupling to the pore domain. *J. Gen. Physiol.* 137:455–472.

25. Shirokov, R. 2011. What's in gating currents? Going beyond the voltage sensor movement. *Biophys. J.* 101:512–514.

26. Labro, A. J., M. F. Priest, …, F. Bezanilla. 2015. Kv3.1 uses a timely resurgent K+ current to secure action potential repolarization. *Nat. Commun.* 6:10173.

27. Cheng, Y. M., C. M. Hull, …, T. W. Claydon. 2013. Functional interactions of voltage sensor charges with an S2 hydrophobic plug in hERG channels. *J. Gen. Physiol.* 142:289–303.

28. Thouta, S., S. Sokolov, …, T. W. Claydon. 2014. Proline scan of the hERG channel S6 helix reveals the location of the intracellular pore gate. *Biophys. J.* 106:1057–1069.

29. Abbruzzese, J., F. B. Sachse, …, M. C. Sanguinetti. 2010. Modification of hERG1 channel gating by Cd2+. *J. Gen. Physiol.* 136:203–224.

30. Goodchild, S. J., and D. Fedida. 2013. Gating charge movement precedes ionic current activation in hERG channels. *Channels (Austin.).* 8:84–89.

31. Piper, D. R., W. A. Hinz, …, M. Tristani-Firouzi. 2005. Regional specificity of human ether-á-go-go-related gene channel activation and inactivation gating. *J. Biol. Chem.* 280:7206–7217.

32. Viloria, C. G., F. Barros, …, P. de la Pena. 2000. Differential effects of amino-terminal distal and proximal domains in the regulation of human *erg* $K^+$ channel gating. *Biophys. J.* 79:231–246.

33. Alonso-Ron, C., P. de la Pena, …, F. Barros. 2008. Thermodynamic and kinetic properties of amino-terminal and S4–S5 loop hERG channel mutants under steady-state conditions. *Biophys. J.* 94:3893–3911.

34. Corbin-Leftwich, A., S. M. Mossadeq, …, C. A. Villalba-Galea. 2016. Retigabine holds KV7 channels open and stabilizes the resting potential. *J. Gen. Physiol.* 147:229–241.

35. Gagnon, D. G., and F. Bezanilla. 2009. A single charged voltage sensor is capable of gating the Shaker $K^+$ channel. *J. Gen. Physiol.* 133:467–483.

36. Morais Cabral, J. H., A. Lee, …, R. MacKinnon. 1998. Crystal structure and functional analysis of the HERG potassium channel N terminus: a eukaryotic PAS domain. *Cell.* 95:649–655.

37. Muskett, F. W., S. Thouta, …, J. S. Mitcheson. 2011. Mechanistic insight into human ether-á-go-go-related gene (hERG) $K^+$ channel deactivation gating from the solution structure of the EAG domain. *J. Biol. Chem.* 286:6184–6191.

38. Ng, C. A., M. J. Hunter, …, J. I. Vandenberg. 2011. The N-terminal tail of hERG contains an amphipathic $\alpha$-helix that regulates channel deactivation. *PLoS One.* 6:e16191.

39. Wang, J., M. C. Trudeau, …, G. A. Robertson. 1998. Regulation of deactivation by an amino terminal domain in human ether-á-go-go-related gene potassium channels. *J. Gen. Physiol.* 112:637–647.

40. Chen, J., A. Zou, …, M. C. Sanguinetti. 1999. Long QT syndrome-associated mutations in the Per-Arnt-Sim (PAS) domain of hERG potassium channels accelerate channel deactivation. *J. Biol. Chem.* 274:10113–10118.